Short communication

Direct melt neutralization and nano-structure of polyethylene ionomer-based nano-composites

Tatsuya Shigemori [a], Masami Okamoto [a,*], Satoshi Yamasaki [b], Hiroshi Hayami [b]

[a] Advanced Polymeric Nanostructured Materials Engineering, Graduate School of Engineering, Toyota Technological Institute, Hisakata 2-12-1, Tempaku, Nagoya 468-8511, Japan
[b] Polymer Materials Technology R&D, Department Electronics & Materials R&D Laboratories, Sumitomo Electric Industries, Ltd., Shimaya, Konohana-ku, 1-1-3, Osaka, 554-0024, Japan

ARTICLE INFO

ABSTRACT

The highly neutralized ionomer-based nano-composite materials were prepared via direct melt processing using zinc oxide (as a neutralizing agent) and organically modified clay. The nano-structure was characterized using wide-angle X-ray diffraction analyses, transmission electron microscopy observations and rheometry. The dispersed organo-clay acted as catalytic sites for the neutralization. From TEM analyses, the nano-sized ionic aggregates with a domain size of approximately 2 nm were randomly arranged in the ionomer matrix. The calculated aggregates density for the nano-composite was 0.08–0.15 nm^{-2}. The temperature-dependent relaxation process observed in the viscoelastic measurements was somehow affected by the presence of the silicate layers, whereas it was strongly affected by the specific interaction via ionic aggregated domains.

© 2008 Elsevier Ltd. All rights reserved.

1. Introduction

Over the last few years, the utility of inorganic nanoscale particles as filler to enhance the polymer performance has been established. Of particular interest is recently developed nano-composite technology consisting of a polymer and organically modified layered filler (organo-clay) because they often exhibit remarkably improved mechanical and various other materials properties as compared with those of virgin polymer or conventional composite (micro/macro-composites) [1–6]. These concurrent property improvements are well beyond what can be generally achieved through the micro/macro-composites preparation.

The synthetic strategy and molecular design was first explored by Toyota group with nylon 6 as the matrix polymer [7]. This new class of material is now being introduced in structural applications, such as gas barrier film and other load-bearing applications [5]. Polymer/clay nano-composites and their self-assembly behaviors have recently been approached to produce nanoscale polymeric materials [1–6]. Additionally, these nano-composites have been proposed as model systems to examine polymer structure and dynamics in confined environments [8–10].

Ionomers consist of random copolymer of ethylene and methacrylic acid (MA) where some of the acid groups are neutralized to form metal (sodium, zinc or magnesium) states [11]. Typically, the MA content of the copolymer is low (<15 mol %), and the degree of neutralization ranges from 20% to 60%. The incorpolation of the ionic groups improves the toughness, melt viscosity, clarity, adhesion properties of the copolymer [11]. In addition, the ionic groups also may offer the possibility of favorable interactions with nano-fillers and promoting intercalation into the nano-galleries [12].

In this communication, and for the first time, we report the preparation and characterization of a highly neutralized type of ionomer-based nano-composite materials via direct melt processing.

2. Experimental part

2.1. Materials

An ionomer resin (Himilan 1706: MA content = 15 wt%, zinc oxide content = 3.70 wt%, neutralization = ~55% and melt flow index (MI) = 4.1 g/10 min) purchased from Du Pont-Mitsui Polychemicals Co., Ltd., was used as a polymer matrix. An organo-clay used in this study was supplied by Southern Clay Products, Inc., and was synthesized by replacing Na^+ ions in montmorillonite (MMT) (cation exchange capacity (*CEC*) of 90 mequiv/100 g, thickness ≈ 1 nm, average length of 150–200 nm) with di-octadecyl di-methylammonium ($DC_{18}DM$) cation by ion exchange.

2.2. Nano-composites preparation

For nano-composites preparation, the organo-clay (powder) and ionomer (pellets) were first dry-mixed by shaking them in a bag. The mixture was then melt extruded using a twin-screw

* Corresponding author.
E-mail address: okamoto@toyota-ti.ac.jp (M. Okamoto).

extruder (PCM-30, Ikegai Corp.) operated at 200 °C (screw speed = 100 rpm, feed rate = 120 g/min) to yield nano-composite strands. The strands were palletized and dried under vacuum at 60 °C for 48 h to remove water. The nano-composite prepared with 20 wt% of organo-clay was denoted as ionomer/clay 20/0/55. The abbreviations of various ionomers and the corresponding nano-composites prepared using zinc oxide (ZnO) (as a neutralizing agent) also are presented in Table 1. For the nano-composites including ZnO, the degree of neutralization exhibits large increment due to the presence of organo-MMT. Presumably, the dispersed organo-clay acts as catalytic sites for the neutralization.

2.3. Characterization

The nano-structure analyses of wide-angle X-ray diffraction (WAXD) and transmission electron microscopy (TEM) were carried out using the same apparatus as in the previous articles [13–15]. To investigate the microscale morphology of the nano-composites, we also used polarizing optical microscope (POM). Because TEM micrograph cover a small area, which might not be entirely representative for the overall microstructure of the sample. The molded sheets were first sandwiched between two pieces of cover glass and placed on a laboratory hot plate at above T_m of matrix ionomer (~120 °C) for 30 s. The molten film was then rapidly put on a thermostatted hot-stage (120 °C) (Linkam RTVMS, Linkam Scientific Instruments, Ltd.) mounted on a POM (Nikon OPTIPHOTO2-POL) [13].

2.4. Melt rheology

Melt rheological measurements were conducted on a RDAII instrument with a torque transducer capable of measurements in the range of 0.2–200 g cm. Dynamic oscillatory shear measurements were performed by applying a time-dependent strain of $\gamma(t) = \gamma_o \sin(\omega t)$ and the resultant shear stress is $\sigma(t) = \gamma_o[G' \sin(\omega t) + G'' \cos(\omega t)]$, with G' and G'' being the storage and loss modulus, respectively. Measurements were conducted by using a set of 25 mm diameter parallel plates with a sample thickness of ~0.8 mm and in the temperature range of 100–180 °C. The strain amplitude was fixed to 2% to obtain reasonable signal intensities even at elevated temperature or low frequency (ω) to avoid the nonlinear response. For each sample investigated, the limits of linear viscoelasticity were determined by performing strain sweeps at a series of fixed ω's. The master curves were generated using the principle of time–temperature superposition and shifted to a common reference temperature (T_{ref}) of 100 °C, which was chosen as the most representative of a typical processing temperature of ionomer.

3. Results and discussion

3.1. Ionomer-based nano-composites formation

WAXD patterns for various ionomers and the corresponding nano-composites are presented in Fig. 1. The profiles were taken

Table 1
Composition and characteristic parameter of ionomers and nano-composites

Samples	ZnO (phr)	Neutralization[b] (%)	Organo-clay (%)
Ionomer 0/55	0	55	0
Ionomer 3/55	3	55	0
Ionomer 6/55	6	55	0
Ionomer 0/83[a]	0	83	0
Ionomer/clay 20/0/55	0	55	20
Ionomer/clay 20/3/74	3	74	20
Ionomer/clay 20/6/89	6	89	20

[a] The sample is prepared using quarternized ammonium salt (QA).
[b] The value measured by titrimetric analysis.
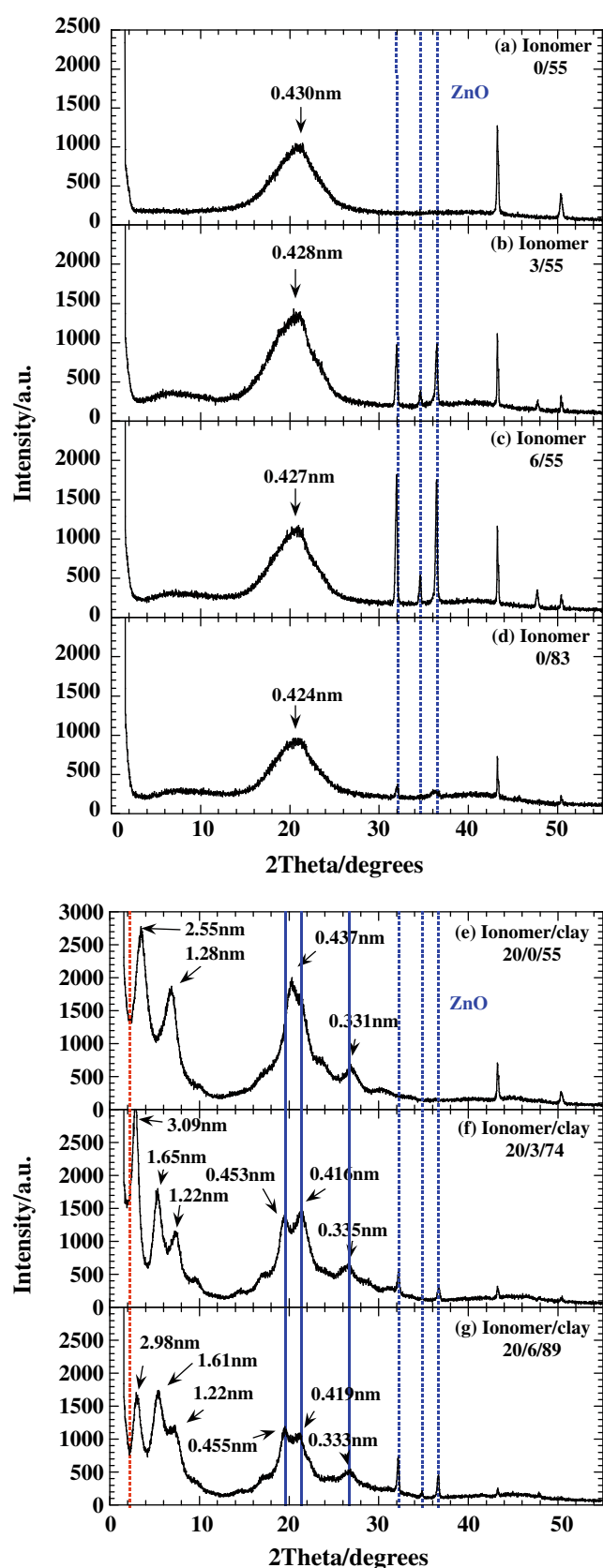
Fig. 1. WAXD profiles of (a) ionomer 0/55, (b) ionomer 3/55, (c) ionomer 6/55, (d) ionomer 0/83, (e) ionomer/clay 20/0/55, (f) ionomer/clay 20/3/74, and (g) ionomer/clay 20/6/89. The dashed line indicates the location of the silicate (0 0 1) reflection of organo-clay (MMT-DC$_{18}$DM). Three dashed lines at $2\Theta = 31 - 37°$ are assigned to the hexagonal crystal of ZnO.

at room temperature. The pattern of ionomer 0/55 matrix (Fig. 1(a)) is displayed here as a baseline to compare the existence of diffraction peaks coming from dispersed MMT layers in the ionomer matrix. In cases of ionomers including ZnO (ionomer 3/55 and 6/55), three sharp peaks are observed at $2\Theta \cong 32.18°$, $34.82°$ and $36.66°$, corresponding to (100), (002) and (101) basal-planes of the dispersed ZnO particles (hexagonal unit cell), respectively, without neutralization reaction in the matrix. These peaks also are observed in the profiles of the nano-composites (Fig. 1(f) and (g)).

The mean interlayer spacing of the (001) plane $(d_{(001)})$ for the MMT intercalated with $DC_{18}DM$ (MMT-$DC_{18}DM$) powder obtained by WAXD measurements is 3.24 nm $(2\Theta \cong 2.72°)$ (indicated with dashed line of Fig. 1(e)–(g)). The strong diffraction peaks at $2\Theta = 15 - 30°$ are assigned to the crystal of ionomer matrix [11].

The appearance of new peaks observed at $2\Theta \cong 3.46°$ $(\cong 2.55 \text{ nm})$, $6.88°(\cong 1.28 \text{ nm})$ for ionomer/clay 20/0/55, were confirmed and these reflection were due to (001) and (002) plane of MMT-$DC_{18}DM$ (Fig. 1(e)). We confirmed that this behavior is essentially the same at any other ionomers upon nano-composite formation (Fig. 1(f) and (g)). Note that the existence of sharp Bragg peak in ionomer-based nano-composites after melt extrusion clearly indicates that the dispersed silicate layers still retain an ordered structure after melt extrusion. Furthermore, the apparent interlayer shrinkage was observed due to the interdigitated layer structure of MMT-$DC_{18}DM$ [16,17]. This phenomenon is deeply discussed in our previous articles [15–17]. Such discussion is beyond the objects of this paper.

We can see a large effect of the dispersed MMT particles on the crystalline structure of the nano-composites (cf. Fig. 1(a) and (e)). The difference in the crystalline structure after neutralization up to 89% is presumably due to the ionic cross-linked structure of the macromolecule chains. The coherent order of the crystalline structure is much higher with increasing degree of the neutralization.

To elucidate the morphologies after preparation of the nano-composites, we conducted POM observation at 120 °C. Ionomer does not contribute to the measured film birefringence because of melting. However, MMT platelets could contribute to the negative birefringence because the refractive index value normal to the basal-plane (001) $(n_{\text{out-of-plane}} = 1.485)$ is smaller than the basal-plane (in-plane) refractive index values $(n_{\text{in-plane}} = 1.505 - 1.550)$ [18].

Fig. 2 shows the morphologies of ionomer-based nano-composites. It is clear from the POM photographs that stacked-and-agglomerated structure of layers is evident in ionomer/clay 20/6/89, while good dispersion appears in ionomer/clay 20/0/55. The internal structure of the nano-composites in the nanometer scale was directly observed via TEM analyses.

Fig. 3 shows the results of TEM bright field images of ionomer/clay 20/0/55, and ionomer/clay 20/6/89, corresponding to the POM experiments, in which dark entities are the cross-section of layered MMT nano-fillers. The figures show both larger views, showing the

dispersion of the MMT within the ionomer matrix, and a higher magnification, permitting the observation of discrete nano-layers. The disorder and delaminated silicate layer structure with the thickness of ∼10 nm is observed in each TEM image. From the TEM it becomes clear that there are some intercalated-and-stacked silicate layers co-existing with the disordered or exfoliated MMT layers in the nano-composite structure. Only the stacked intercalated silicate layers are responsible for very sharp WAXD reflection as observed in Fig. 1(e)–(g), whereas the disordered or exfoliated silicate layers have no periodic stacking and thus remain WAXD silent. Actually, there is a large anisotropy of the stacked silicate layers. The size of the some of the stacked silicate layers appears to reach about 100–150 nm in lengths. Typically the large-in lateral size-MMT layers create stacked intercalated structure, whereas the smaller layers tend to exfoliate [19]. A significant difference in the TEM images among the degree of neutralization is not observed.

In Fig. 3, the dark areas represent the nano-sized ionic aggregates similar to what is observed for other ionomers [20]. After a close look, shown in the enlarged views, we clearly observe spheres with a domain size of approximately 2 nm (indicated with arrows). The ionic aggregates are randomly arranged in the ionomer matrix. The number of the aggregates (N_{ion}) can be estimated from the enlarged images. The calculated value of N_{ion} was 0.08–0.12 nm^{-2} for ionomer/clay 20/0/55 and 0.98–0.15 nm^{-2} for ionomer/clay 20/6/89. This result suggests that the ionic cross-linked density in the system of 20/6/89 is higher than that of matrix in the absence of ZnO (6 phr).

3.2. Melt rheology

Generally, the rheology of polymer melts strongly depends on the temperature at which measurement is carried out. It is well known that for the thermo-rheological simplicity, isotherms of storage modulus $(G'(\omega))$, loss modulus $(G''(\omega))$ and complex viscosity $(|\eta^*|(\omega))$ can be superimposed by horizontal shifts along the frequency axis [21]:

$$b_T G'(a_T\omega, T_{\text{ref}}) = b_T G'(\omega, T); \quad b_T G''(a_T\omega, T_{\text{ref}}) = b_T G''(\omega, T);$$
$$|\eta^*|(a_T\omega, T_{\text{ref}}) = |\eta^*|(\omega, T)$$

where a_T and b_T are the frequency and vertical shift factors, respectively. T_{ref} is the reference temperature. All isotherms measured for ionomers and for various nano-composites can be superimposed along the frequency axis.

The master curves for $G'(\omega)$ and $G''(\omega)$ of ionomer 0/83 and ionomer/clay 20/6/89 are presented in Fig. 4. At all frequencies, both $G'(\omega)$ and $G''(\omega)$ for nano-composite (20/6/89) increase monotonically with increasing silicate loading compared with that of ionomer (0/83). At low frequencies $(a_T\omega < 10^{-2} \text{ rad/s})$, both moduli exhibit week frequency dependence in the presence of organo-clay that means there is a gradual change of behavior from liquid like to solid like.

Fig. 2. Polarized optical micrographs of (a) ionomer/clay 20/0/55, (b) ionomer/clay 20/3/74, and (c) ionomer/clay 20/6/89. All micrographs were taken at 120 °C just after annealing for 30 s.
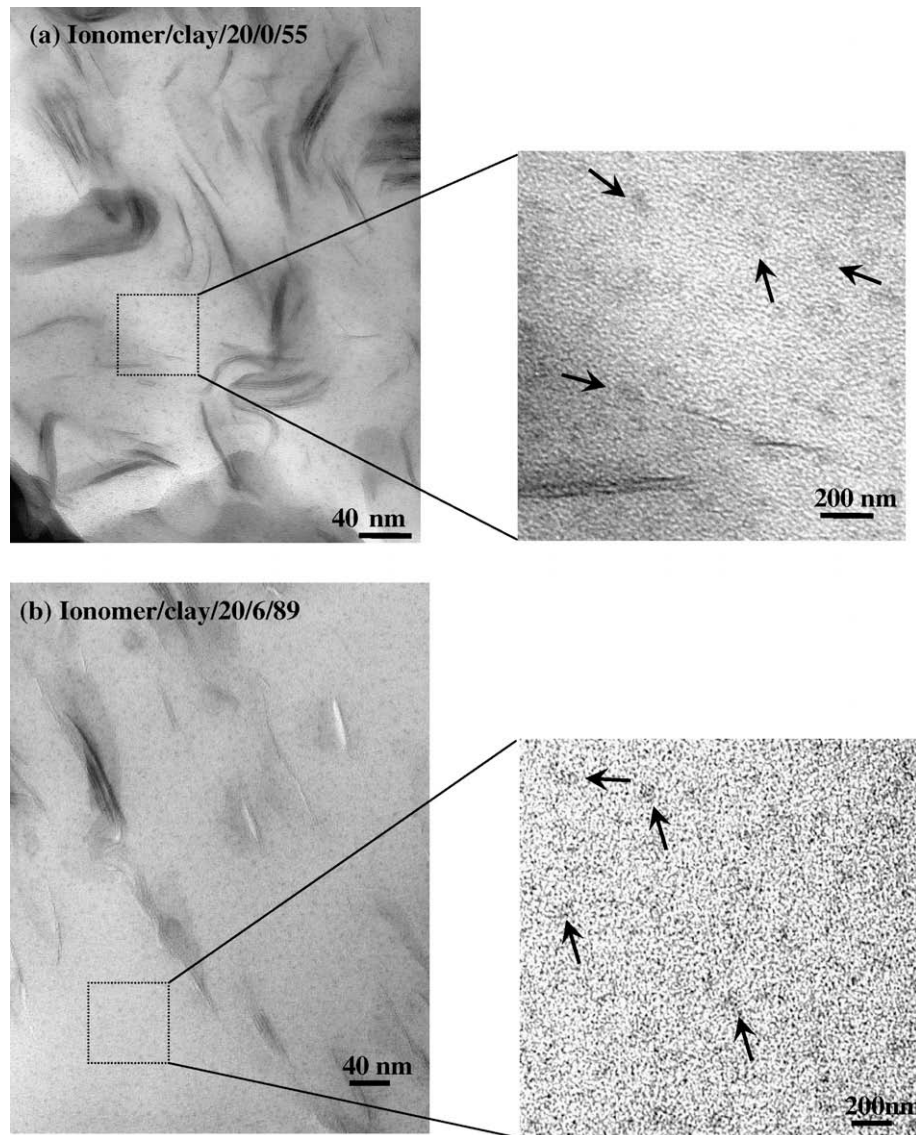
Fig. 3. Bright field TEM images of (a) ionomer/clay 20/0/55 and (b) ionomer/clay 20/6/89. The dark entities are cross-section and/or face of intercalated-and-stacked silicate layers, and the bright areas the matrix. The enlarge parts shown are from the nano-sized ionic aggregates in the original images.

The terminal zone slope values of both ionomers and nano-composites are estimated at lower $a_T\omega$ region (<10^{-1} rad/s). The slopes of $G'(\omega)$ and $G''(\omega)$ are significantly lower for all nano-composites compared to that of ionomers. The lower slope values and the higher absolute values of the dynamic moduli indicate the formation of "spatially-linked" structure (also observed from TEM photograph, see Fig. 3) in the nano-composites under molten state [22,23]. This type of prevented relaxation due to the highly geometric constraints of the stacked and intercalated silicate layers leads to the presence of the pseudo-solid like behavior as observed in MMT-based polymeric nano-composites [24].

3.3. Relaxation time

To understand the generic dynamic rheology, the presence of a plateau in $G'(\omega)$ in the master curve of the dynamic frequency sweep enables one to predict an entanglement molecular weight (M_e) using the following equation [21]:

$$M_e = \frac{\rho RT}{G_N^0} \tag{1}$$

where ρ is the polymer density (= 0.800 g/cm^3), an G_N^0 is the plateau modulus which is determined from the measured $G'(\omega)$ when tan δ is at a minimum [25], and RT is the thermal energy. In this study, M_e corresponds to the interchain entanglement between ionic aggregated domains in the melts, and is a measure of the flexibility of the polymer chains.

Table 2 shows the results at a reference temperature of 100 °C. For the nano-composite melts, M_e decreases due to the presence of organo-clay particles. Likewise, when the degree of neutralization is increased, the value also decreases, reflecting the decreased flexibility of the materials.

We investigated the low frequency values of η^* as a function of temperature in each system. At temperature where a zero-shear value was not obtained experimentally, a combination of time–temperature superposition and fitting using the Ellis model was employed to obtain a zero-shear viscosity (η_0^*) from a master curve. The Doi-Edwards theory predicts a longest relaxation time (λ_d) associated with diffusion out of the tube as

$$\lambda_d = \frac{15}{\pi^2} \frac{\eta_0^*}{G_N^0} \tag{2}$$
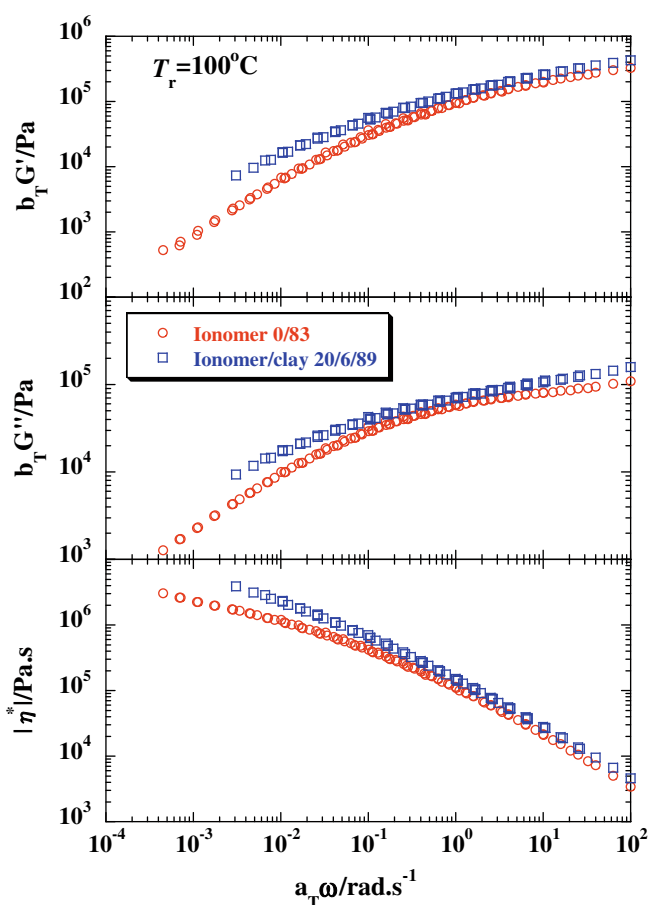
Fig. 4. Reduced frequency dependence of storage modulus ($G'(\omega)$), loss modulus ($G''(\omega)$), and complex viscosity ($|\eta^*|(\omega)$) of ionomer 0/83 and ionomer/clay 20/6/89 at $T_{ref} = 100\,^\circ C$.

Table 2
Molecular weight between entanglements M_e at a reference temperature of 100 °C

Samples	M_e (g/mol)
Ionomer 0/55	9600
Ionomer 3/55	12,400
Ionomer 6/55	18,100
Ionomer 0/83	7600
Ionomer/clay 20/0/55	6900
Ionomer/clay 20/3/74	7300
Ionomer/clay 20/6/89	5800

We can determine a polymer characteristic time in each system. There is a significant increase of λ_d for ionomer/clay 20/6/89 with enhancement of the neutralization as compared with that of ionomer/clay 20/0/55 (see Fig. 5). Therefore, with increasing the degree of neutralization, λ_d increases as expected.

4. Conclusions

We have successfully prepared ionomer/organically modified layered silicate nano-composite via simple melt extrusion of ionomer and MMT-DC$_{18}$DM, wherein silicate layers of the clay were intercalated, stacked ($\sim$10 nm thickness), and nicely distributed in the ionomer matrix. For the nano-composites including ZnO, the degree of neutralization exhibited large increment as compared with system in the absence of organo-clay. The dispersed organo-clay acted as catalytic sites for the neutralization. At this
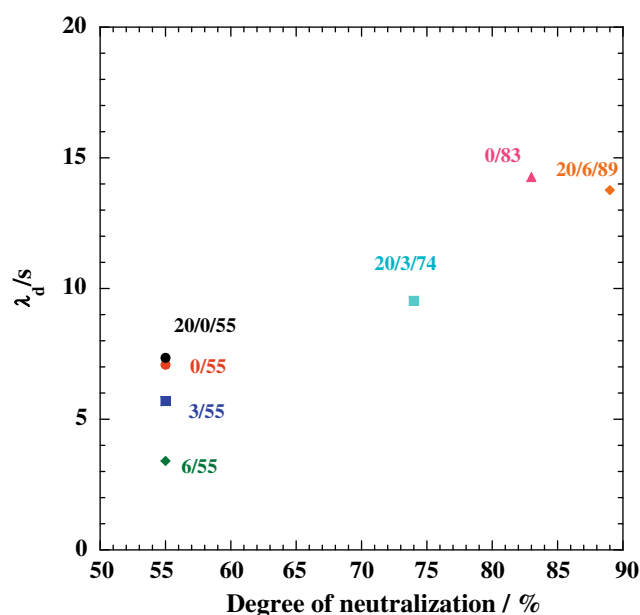
Fig. 5. Characteristic relaxation time (λ_d) versus the degree of neutralization.

moment, we are not able to propose the real mechanism of the catalytic effect. The effect will be clarified shortly.

We observed a large effect of the dispersed MMT particles on the crystalline structure of the nano-composites. The difference in the crystalline structure after neutralization up to 89% was presumably due to the ionic cross-linked structure of the macromolecule chains. The coherent order of the crystalline structure was much higher with increasing degree of the neutralization. From TEM analyses, the nano-sized ionic aggregates with a domain size of approximately 2 nm were randomly arranged in the ionomer matrix. The calculated aggregates density for the nano-composite was 0.08–0.15 nm^{-2}.

The dependence of the frequency shift factors on the organo-clay loading suggested that the temperature-dependent relaxation process observed in the viscoelastic measurements was somehow affected by the presence of the silicate layers, whereas it was strongly affected by the specific interaction via ionic aggregated domains. The characteristic relaxation time significantly increased for ionomer/clay 20/6/89 with enhancement of the neutralization as compared with that of ionomer/clay 20/0/55.

Acknowledgment

References

[1] Sinha Ray A, Okamoto M. Polymer/layered silicate nanocomposites: a review from preparation to processing. Prog Polym Sci 2003;28:1539–641.
[2] Vaia RA, Wagner HD. Framework for nanocomposites. Mater Today 2004;7:32–7.
[3] Gao F. Clay/polymer composites: the story. Mater Today 2004;7:50–5.
[4] Okamoto M. Recent advances in polymer/layered silicate nanocomposites: an overview from science to technology. Mater Sci Technol 2006;22:756–79.
[5] Okada A, Usuki A. Twenty years of polymer–clay nanocomposites. Macromol Mater Eng 2006;291:1449–76.
[6] Hussain F, Hojjati M, Okamoto M, Gorga RE. Review article: polymer-matrix nanocomposites, processing, manufacturing, and application: an overview. J Compos Mater 2006;40:1511–75.
[7] Usuki A, Kojima Y, Okada A, Fukushima Y, Kurauchi T, Kamigaito O. Swelling behavior of montmorillonite cation exchanged for omega-amino acids by epsilon-caprolactam. J Mater Res 1993;8:1174–8.
[8] Vaia RA, Giannelis EP. Polymer melt intercalation in organically-modified layered silicates: model predictions and experiment. Macromolecules 1997;30:8000–9.

[9] Krishnamoorti R, Vaia RA, Giannelis EP. Structure and dynamics of polymer–layered silicate nanocomposites. Chem Mater 1996;8:1728–34.

[10] Rao Y, Pochan JM. Mechanics of polymer–clay nanocomposites. Macromolecules 2007;40:290–6.

[11] Eisenberg A, Kim JS. Introduction to ionomers. New York: Wiley; 1998.

[12] Bhiwankar NN, Weiss RA. Melt-intercalation of sodium-montmorillonite with alkylamine and quarternized ammonium salts of sulfonated polystyrene ionomers. Polymer 2005;46:7246–54.

[13] Saito T, Okamoto M, Hiroi R, Yamamoto M, Shiroi T. Poly(p-phenylenesulfide)-based nano-composite formation: dealmination of organically modified layered filled via solid-state processing. Polymer 2007;48:4143–51.

[14] Nam PH, Maiti P, Okamoto M, Kotaka T, Hasegawa N, Usuki A. A hierarchical structure and properties of intercalated polypropylene/clay nanocomposites. Polymer 2001;42:9633–40.

[15] Yoshida O, Okamoto M. Direct intercalation of polylactide chains into nano-galleries: interlayer expansion and nanocomposite structure. Macromol Rapid Commun 2006;27:751–7.

[16] Saito T, Okamoto M, Hiroi R, Yamamoto M, Shiroi T. Intercalation of diphenyl sulfide into nanao-galleries and preparation of poly(p-phenylenesulfide)-based nano-composites. Macromol Mater Eng 2006;291:1367–74.

[17] Yoshida O, Okamoto M. Direct melt intercalation of polymer chains into nano-galleries: interdigitated layer structure and interlayer expansion. J Polym Eng 2006;26:919–39.

[18] Greene KR. Clay Miner 1970;8:405.

[19] Sinha Ray S, Yamada K, Okamoto M, Ogami A, Ueda K. New polylactide/layered silicate nanocomposites. 3. High-performance biodegradable materials. Chem Mater 2003;15:1456–65.

[20] Lefelar JA, Weiss RA. Concentration and counterion dependence of cluster formation in sulfonated polystyrene. Macromolecules 1984;17:1145–7.

[21] Utracki LA. Polymer alloya and blends: thermodynamics and rheology. NY: Hasser Publishers; 1990.

[22] Sinha Ray S, Maiti P, Okamoto M, Yamada K, Ueda K. New polylactide/layered silicate nanocomposites. 1. Preparation, characterization, and properties. Macromolecules 2002;35:3104–10.

[23] Ren J, Silva AS, Krishnamoorti R. Linear viscoelasticity of disordered polystyrene–polyisoprene block copolymer based layered-silicate nanocomposites. Macromolecules 2000;33:3739–46.

[24] Hoffmann B, Kressler J, Stoppelmann G, Friedrich C, Kim GM. Rheology of nanocomposites based on layered silicates and polyamide-12. Colloid Polym Sci 2000;278:629–36.

[25] Wu S. Chain structure and entanglement. J Polym Sci Part B Polym Phys 1989;27:723–41.